2018-06-15

Study of interaction of chitosan with Fluoride

Wagutu, Agatha W.

Biointerface Research in Applied Chemistry

Study of Interaction of Chitosan with Fluoride

Article · June 2018

CITATION
1

READS
234

3 authors:

Agatha Wagutu
Kirinyaga University
11 PUBLICATIONS **32** CITATIONS
SEE PROFILE

Tatiana Pogrebnaya
The Nelson Mandela African Institute of Science and Technology
50 PUBLICATIONS **99** CITATIONS
SEE PROFILE

Revocatus L. Machunda
The Nelson Mandela African Institute of Science and Technology
41 PUBLICATIONS **296** CITATIONS
SEE PROFILE

Volume 8, Issue 3, 2018, 3170 - 3177 ISSN 2069-5837

Biointerface Research in Applied Chemistry

www.BiointerfaceResearch.com

Original Research Article Open Access Journal

Received: 27.04.2018 / Revised: 15.05.2018 / Accepted: 30.05.2018 / Published on-line: 15.06.2018

Study of interaction of chitosan with Fluoride

Agatha W. Wagutu [1, 3, *], Tatiana Pogrebnaya [1], Revocatus Machunda [2]

[1] Department of Materials and Energy Science and Engineering, Nelson Mandela African Institution of Science and Technology, P.O.BOX 447, Arusha, Tanzania
[2] Department of Water, Environmental Science and Engineering, Nelson Mandela African Institution of Science and Technology, P.O.BOX 447, Arusha, Tanzania
[3] Department of Chemistry, Mwenge Catholic University, P.O. Box 1226, Moshi, Tanzania

*corresponding author e-mail address: ***awagutu@gmail.com***

ABSTRACT

Interaction of chitosan with fluoride (F^-) has been studied using experimental and computational methods. Chitosan was extracted from prawns shells and modified by cross-linking with glutaraldehyde and protonation using concentrated hydrochloric acid. Modified and pristine chitosan were characterized using XRD, FT-IR and UV–Vis. Adsorption of F^- from solution was determined using ion selective electrode meter. β-$_D$-glucosamine (β-GlcN) monomer was used to model chitosan. Optimization of molecular geometry, harmonic vibrations analysis and interaction energies with fluoride were computed using DFT with B3LYP/ 6-311**G (d,p) level of theory. Electronic absorption spectra of β-GlcN was calculated by Time Dependent–DFT using the same level of theory and compared with UV-VIS spectra of pristine chitosan. Firefly 8.1.1 program package was used for all computations. Computed IR frequencies were assigned using Chemcraft visualization software and compared with experimental FT-IR spectra of chitosan and literature values. Equilibrium geometry calculated was compared with X-ray diffraction. Results indicated that computed parameters matched well with experimental results and confirmed that electropositivity hydrogen atoms of amine and its adjacent hydroxyl groups in chitosan influenced the adsorption of fluoride from solution by electrostatic attraction also, that protonation of the amine group increased adsorption capacity significantly.

Keywords: *Chitosan; DFT; Fluoride; Glucosamine; FT-IR; XRD*

1. INTRODUCTION

Chitosan is a naturally occurring copolymer of $_D$-glucosamine (GlcN) and N-acetyl-$_D$-glucosamine (GlcNac) which are joined by β-(1,4)-glycosidic bonds. Commercially, chitosan is obtained by alkali hydrolysis of chitin, which can be extracted from exoskeleton of insects, crustaceans or from fungi [1]. Due to its pseudo polycationic and chelating properties, chitosan has been shown to interact well with anionic particles and microbial cell membrane [2-6]. This, in addition to being biodegradable, biocompatible and non-toxic has enabled its applications in fields of environmental remediation, biomedicine, food packing and agriculture [7-10]. Investigation of how chitosan and its derivatives interact with charged particles and surfaces is thus deemed fundamental in determination of the mechanism, the structure and stability of complexes formed in the environments [11, 12].

Worldwide, fluoride (F^-) is one of the key anionic contaminants in drinking water with profound dental and skeletal health risks. A concentration of 1.5-4 mg/L can trigger dental fluorosis while ranges of 4-10 mg/L over prolonged exposure can progress to skeletal fluorosis and increase susceptibility to other risks such as renal diseases, cancer and neurological damage [13-15]. In fluoride endemic regions defluoridation of drinking water is required, to mitigate and control the occurrence of fluorosis [16, 17]. Various technologies and adsorbents have been studied and applied in adsorption of F^- from water of varying concentrations. Among them, chitosan has been given significant attention as a sustainable biosorbents in low F^- concentrated water [12, 18]. Chitosan application is however, limited due to its poor stability in acidic environments. Hence, it requires to be modified into a stable form before effective use. Cross-linking chitosan with glutaraldehyde or other agents have been found to enhance stability in acidic and alkaline environments [19, 20].

Several experimental studies on the interactions of chitosan and its derivatives with F^- are available in the literature [21-25]. However, only a few computational studies explain the theory, mechanism and favorable sites of binding of F^- ions onto chitosan [26]. The present study thus aimed to investigate the interaction of F^- ions with pristine and protonated chitosan using experimental and DFT methods, with focus on the structure, reaction mechanism, and stability of the complex formed and the efficiency of adsorption.

2. EXPERIMENTAL SECTION

2.1. Experimental details

2.1.1. Extraction of chitosan (CHS) from prawns shells. Chitosan was extracted from white prawns (*Fenneropenaeus indicus*) shells following procedure described in literature [27, 28] with slight modifications. In brief, clean and dry shells were ground into 2 mm sizes and deproteinated using 0.25 M NaOH at 70 °C for 2h. The protein free shells were washed with water to neutral pH followed by drying in hot air oven at 50 °C for 12 h. Dry shells were treated with 2 M HCl (solid to acid ratio = 1: 4) at room temperature for 24 h. The residue (chitin) was rinsed to neutral

pH, then treated with 1% potassium permanganate ($KMnO_4$) ratio 1:5 for 2 h, followed by 3% oxalic acid for 3 hrs to obtain decolorized chitin. De-acetylation of chitin was carried out using 50% NaOH at 70-75 °C for 24 h with constant stiring. Chitosan obtained was rinsed with de-ionized water to neutral pH and oven dired in hot air for 12 h at 50 °C. To obtain purified chitosan, a solution of chitosan in 1% acetic acid was precipitated with 0.25 M NaOH, followed by rinsing and freeze drying.

2.1.2 Preparation of protonated cross-linked chitosan (PCCs). PCCs was prepared by dissolving 3 g CHS powder in 150 ml of 1 % acetic acid, 20-25 ml of the solution was coated onto glass Petri dish with diameter 8-10 cm to form thin films which were then dried in a forced air oven at 50 °C for 6 h. The surface of the dry films was treated with 0.1M NaOH and allowed to stand for 2 h for the films to separate. Wet films were washed with warm distilled water until the rinse water attained a neutral pH and then dried at 50 °C. Dry films were cross-linked with 2.5 % glutaraldehyde (GA), ratio of 1g/25 ml for 24 h at 50 °C. The cross-linked films were then rinsed to remove excess GA, dried and treated with concentrated HCl for 30 min at room temperature [21]. PCCs obtained was thoroughly rinsed with distilled water to neutral pH, oven dried and reduced into powder for F^- adsorption tests.

2.1.3 Characterization of CHS and PCCS. XRD patterns of chitosan samples was determined using Bruker D2 PHASER bench-top diffractometer with monochromatized CuKα radiation (λ= 0.15406 *nm*) over 2θ range of 3 -75 ° at a scanning speed of 3° per minute and a step size of 0.02°. Diffraction data were analyzed using EXPO 2014 software for peak indexing, space group determination and estimation of the reflection intensities [29]. Infrared spectra analysis was conducted under vacuum at room temperature using attenuated total reflectance (ATR) with ZnSe crystal as reflection element on a Bruker Tensor 27 Fourier transform infrared (FT-IR) spectrometer in the range of 4000 - 400 cm^{-1} at a resolution of 2 cm^{-1}. UV-Vis absorbance of chitosan solution, 10 mg /25 ml of 0.1 M HCl, was measured using UNICO SQ-2800 single beam spectrophotometer in the range 190-230 nm. Elemental analysis was done using Flash 2000 CHNS/O analyzer (Thermo Scientific). Degree of deacetylation (DDA) was calculated from CHNS data by relating weight percent of elemental carbon to nitrogen following Eq (1) [30] and further verified by FT-IR spectroscopy using the relation between intensities of reference band at 1420 cm^{-1} and amide band at 1320 cm^{-1} Eq (2), as described in literature [31, 32].

$$DDA\% = (6.857 - C/N)/1.714 \quad (1)$$

where: C/N is the ratio of carbon : nitrogen obtained by elemental analysis

$$A1320/A1420 = 0.3822 + 0.03133DA \quad (2)$$

where: A1320/A1420 is the ratio of absorption intensity bands at 1320 and 1420 cm^{-1} and DA is degree of acetylation and it is equivalent to 100% - DDA% .

2.1.4 F^- Batch adsorption tests. Adsorption experiments were conducted in triplicate using 0.25 g of chitosan adsorbent mixed with 50 ml of fluorinated water of concentration 10.4 mg/L. The mixtures were shaken in 250 ml plastic bottles using a Retch AS 200 shaker with amplitude set at 70 for 12 h. Final pH and residue F^- concentration was determined using ion selective electrode. Adsorption capacity was calculated using Eq (3).

$$Q_e = C_0 - C_e)\ V/M \quad (3)$$

where Q_e is the F^- adsorbed at equilibrium (mg/g), C_0 is initial F^- concentration (mg/L), C_e is F^- concentration at equilibrium (mg/L), V is the volume of water (L) and M is mass of adsorbent (g).

2.2 Computational Details. Avogadro (1.1.0) program [33] was used to generate structures and coordinates of GlcN molecule and adducts. Molecular mechanics simulations using Open Babel's force fields (OBForceField MMFF94) provided within Avogadro package was used for conformational search with systematic rotor search function. Lowest energy conformers were selected for DFT study. Firefly quantum chemical package, version 8.1.1 [34] partially based on the GAMESS (US) source code [35] was employed in DFT calculations. Molecular structures were fully optimized at the B3LYP/ 6311**G (d,p) level of theory without any symmetry restrictions [36, 37].

Stationary points of molecular potential energy surface were characterized using analytical harmonic vibrational analysis for optimized structures at the same level of theory. Absence of imaginary frequencies confirmed that stationary points corresponded to minima on the energy surface [38]. For characterization of excited state properties, Time-Dependent-DFT calculation was employed to obtain the electronic spectra for gas phase and solvent phase using polarizable continuum model (PCM). Visualization of optimized structures, spectra and assignment of vibrational modes was done using ChemCraft graphical program [39].

3. RESULTS SECTION

3.1 Properties of CHS, PCCs and GlcN

3.1.1 Structure analysis. Average recovery of CHS from prawns shells was 16% on a dry basis and elemental composition as follows; C 36.25%, H 6.04%, N 6.75%. DDA obtained from elemental analysis, 86.7% and FT-IR analysis 80.2%, seemed not to differ significantly, the average value, 83.5% was accepted as final DDA of CHS. This value indicated that most acetyl groups were removed from the molecular chain of chitin leaving behind chitosan with more free and chemically reactive amino groups.

XRD patterns of CHS and protonated cross-linked chitosan (PCCs) are shown in Fig 1. Diffraction peaks were observed at 2θ position; 9.6, 12.3, 19.6 and 26.5°. Broad intense peaks at 2θ = 19.6°, indexed as 002 is characteristics of anhydrous chitosan and associated with mixture of semicrystalline and amorphous phases. Two low intensity peaks in lower 2θ values (9.6 and 12.3°) indicate little hydrated crystalline phases were present in the samples [40]. The sharp medium peak at 2θ = 26.5°, indexed as 300 is presumed to indicate the presence of highly

crystalline chitin in the samples, given that DDA of chitosan was about 83%. For PCCs, 002 peak weakened and became broader while the 300 peaks remained sharp with reduced intensity. The

This loss of crystallinity in cross-linked chitosan biopolymer has also been reported [21, 41, 42]. For both CHS and PCCs, the peaks were indexed as triclinic unit cell with lattice parameters as shown in Table 1. Parameters of CHS corresponds well to those obtained for monoclinic structure in [43]. Increase in axial lengths and cell volume in PCCs as compared to CHS indicate more molecules of chitosan and GA are packed in the unit cell after cross-linking.

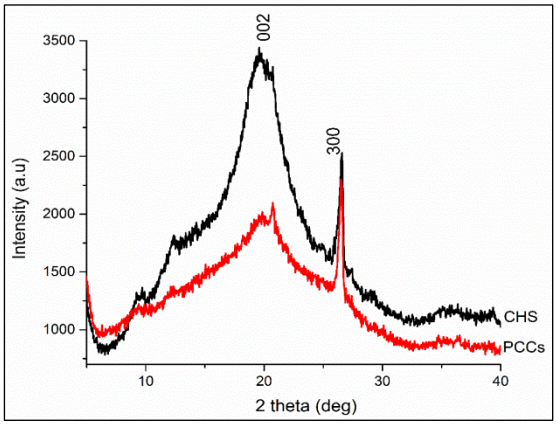

Fig. 1. XRD pattern of CHS (upper curve) and PCCs (lower curve).

Table1. Lattice parameters of CHS and PCCs refined cells

Lattice parameter	CHS	PCCs	CHS literature [43]
Crystal Family	Triclinic	Triclinic	Monoclinic
Space-Group	P-1	P-1	P21
A (Å)	9.679	12.134	9.46
B (Å)	9.829	14.365	9.79
C (Å)	10.885	17.994	10.46
Alpha (°)	102.3	66.7	-
Beta (°)	107.5	77.6	105.3
Gamma (°)	92.9	80.9	-
Volume ($Å^3$)	957.7	1795.8	957.0

From theoretical analysis, two energetically favored conformers of GlcN, alpha (α-) and beta (β-) each with $^4C_1$ chair configuration were found through conformational search. The β-conformer had lower energy (-14.44 $kJmol^{-1}$) than the α-conformer, thus is considered more stable. The main difference between the structures of α- and β-conformer is the orientation of OH group attached to carbon C1 and the H atoms attached to N1 atom, Fig 2.

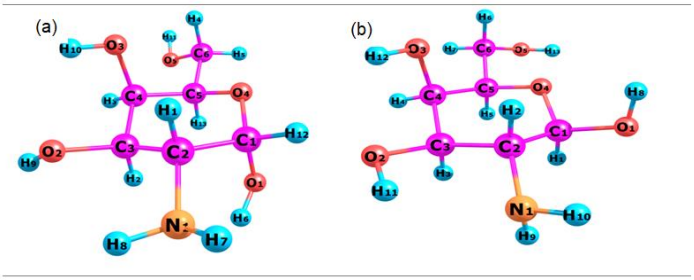

Fig. 2. Conformers of GlcN: (a) α- conformer, E= -667.5315 a.u, (b) β-conformer, E= -667.5370 a.u.

loss in crystallinity of 002 peak can be explained by possible loss of H-bonding upon interaction of GA with amine groups of CHS.

Further analysis of β-GlcN identified three stable rotamers; I - Gauche (G^+g^-), II - Gauche (G^-g^-) and III- Trans (Tg^-) (Fig. 3). These rotamers are defined by O5-C6-C5-O4 and H13-O5-C6-C5 dihedral angles in Newman projection as described in [44, 45]. Selected geometrical parameters; bond lengths, valence angles and torsion angles for α- and β-GlcN for gas phase are compared with those of β-GlcN for solvent phase (water) computed by PCM model and those obtained by XRD analysis of CHS, Table 2. The bond lengths in α- and β-GlcN molecules are typical values for C-O, C-C, C-N and O-H within the range of 1.43, 1.54, 1.47 and 0.96 Å, respectively. Bond angles with C atom in vertex and C-O-H are close to tetrahedral and the pyranose ring is nonplanar. No significant difference was observed in structural parameters between the gas phase and solvent phase. Parameters obtained from XRD analysis of CHS are within the same range compared to theoretical parameters. β-rotamer I, was selected for the study of interaction with F^- and comparison with CHS.

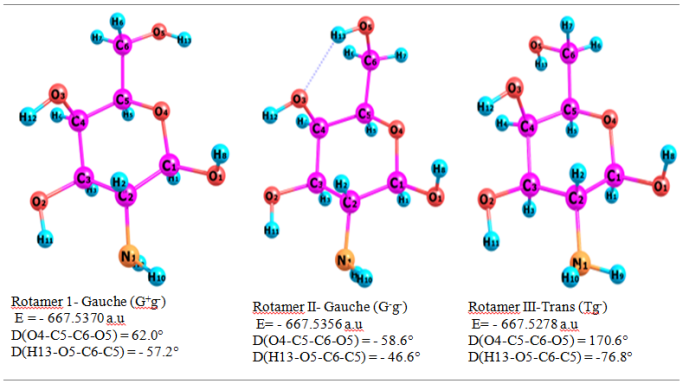

Fig. 3. Optimized structures of the three rotamers of β-D-glucosamine.

Table 2. Geometry comparison of α- and β-GlcN (lowest energy monomers) with XRD parameters of CHS.

	Bond Length-6311 (Å)			
	α-GlcN- gas	β-GlcN - gas	β-GlcN - PCM	XRD CHS solid
R(C1-C2)	1.547	1.540	1.535	1.546
R(C2- N1)	1.470	1.463	1.465	1.537
R(C3-O2)	1.442	1.422	1.436	1.493
R(O2-H9)	0.963	-	-	
R(O2-H11)	-	0.969	0.965	
R(C1-O4)	1.399	1.419	1.424	
R(C1- O1)	1.415	1.398	1.399	
R(O1-H6)	0.971	-	-	
R(O1-H8)	-	0.966	0.968	
R(C4-O3)	1.423	1.420	1.427	
R(O3-H10)	0.965	-	-	
R(O3-H12)	-	0.966	0.968	
Bond Angles (°)				
A(C1-C2-N1)	108.5	115.7	109.7	118.2
A(C3-O2-H9)	108.9	-	-	
A(C3-O2-H11)	-	106.0	108.8	
A(C1-O1-H6)	105.5		-	
A(C1-O1-H8)	-	107.5	108.4	
A(C4-O3-H10)	107.0	-		
A(C4-O3-H12)	-	106.4	106.6	
A(O4-C5-C6)	106.0	107.8	106.5	112.6
A(C1-O4-C5)	113.9	115.0	113.6	
Dihedral Angles (°)				
D(C2-C1-O1-H6)	32.1			
D(C2-C1-O1-H8)		-73.6		
D(C2-C3-C4-C5)	53.7	52.3	51.2	50.9
D(O4-C5-C6-O5)	177.2	62.0	62.7	

3.1.2 Vibrational spectra of β GlcN and CHS powder. Theoretical IR spectra of β-GlcN for gas phase and solvent phase confirmed the optimized structures were in the most stable state, by the

absence of imaginary frequency. Comparison with FT-IR spectra of CHS is given in Fig.4. IR Modes for CHS agree well with values reported in literature [46, 47]. In all cases, highest intensity bands at 1050-1170 cm^{-1} were related with of C-O-C and C-O bonds stretching. Band at 1667cm^{-1} represented free NH_2 bending in β GlcN. For CHS this band was observed at shorter wavenumbers, 1595 cm^{-1} very close to C=O band seen at 1657 cm^{-1}, indicating the presence of acetyl group since the CHS was partially deacetylated (DDA=83.5%). Characteristic CH and NH stretching bands were observed at 2900-3100 cm^{-1} and 3200-3500 cm^{-1} respectively. FT-IR modes for CHS differed slightly with those of β-GlcN for gas phase and solvent phase due to the presence of acetyl groups and intermolecular forces in the solid from. For instance, the CH, NH_2 and OH stretching modes around 3000-3700 are all shifted to shorter wavenumbers in CHS

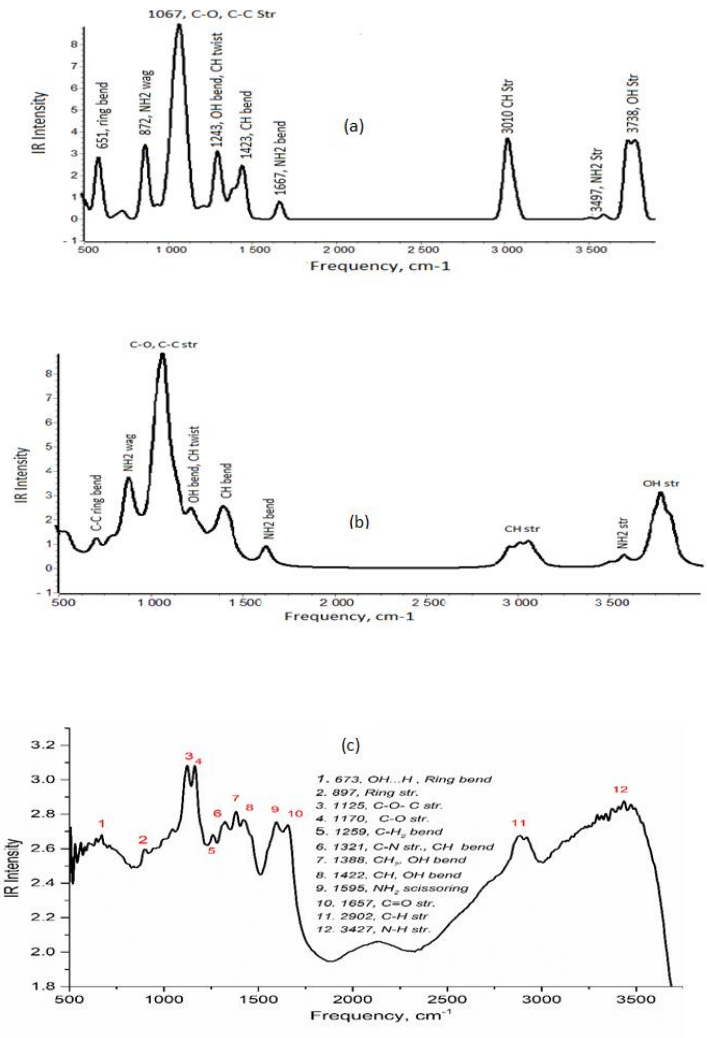

Fig. 4. IR spectra of β-GlcN for gas phase (a) solvent (water) phase (b) and FT-IR of CHS powder (c).

3.1.3 UV-Vis spectra of β-GlcN (gas phase, solvent phase) and CHS powder. UV-VIS spectra of β-GlcN for gas phase, solvent phase, and CHS powder are shown in Fig. 5. Absorption peaks of β-GlcN for the solvent phase are shifted to shorter wavelength compared to gas phase adsorptions. Two peaks identified for CHS, (206 and 217 nm) are comparable to peaks at 205 and 214 nm in β-GlcN for gas phase but differs slightly from that reported in literature [48], which measured absorption maxima at 201 nm for pure chitosan and admixture of GlcNac and GlcN in a solution of 0.1M HCl.

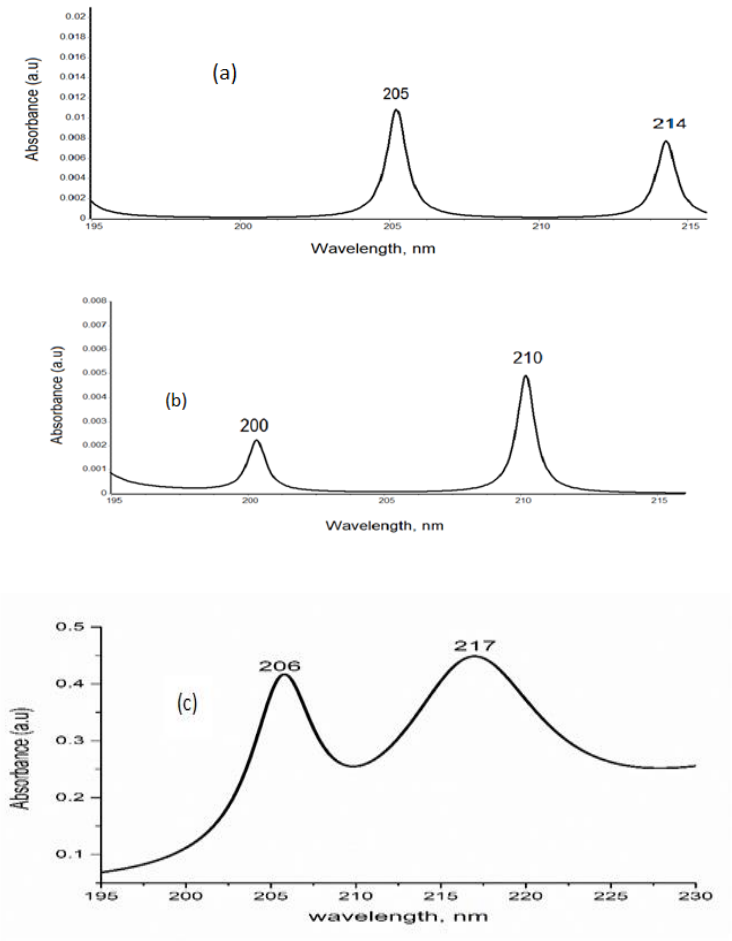

Fig. 5. Electronic absorption spectra of β-GlcN for gas phase (a) solvent (water) phase (b) and UV-Vis of CHS powder (c).

3.2 Analysis of protonated β-GlcN and PCCs. Geometric optimized structure, charge distribution, and dipole moment (μ) of protonated glucosamine (β-GlcN-H^+) is shown in Fig 6, in comparison with its unprotonated form. Proton affinity, calculated from Eq (4) was found to be -943 kJ mol^{-1} (-225 kcal mol^{-1}) which coincides with that reported by *Fattahi et al* (- 225 kcal mol^{-1}) [49]. A significant change in μ and charge distribution of atomic sites was observed after protonation. This change relates mostly to atoms and bonds of the amine group and surroundings and is manifested in slight changes in bond length and bond angles. As seen from Tables 2, 4, C-N bond length increased by 0.05 Å, ring C-O bond decreased with 0.04 Å while C-C-N bond angle decrease by 4.7° and the rest of the angles increased with 1-4° in β-GlcN-H^+.

$$\beta\text{-GlcN} + H^+ \longrightarrow \beta\text{-GlcN-}H^+ + \Delta rE \qquad (4)$$

IR spectra of β-GlcN-H^+ (Fig 7) indicate significant changes in the frequency modes as a result of protonation. The peaks at 651 and 872 cm^{-1} representing GlcN ring bending and NH_2 vibration disappeared completely in the protonated adduct. Two new peaks at 924 and 1487 cm^{-1} representing vibration of NH_3^+ group were observed, while the intensity of NH_2 band at 3400 - 3500 cm^{-1} increased considerably. All CH vibrations are weaker in β-GlcN-H^+ as compared to β-GlcN (Fig 4a).

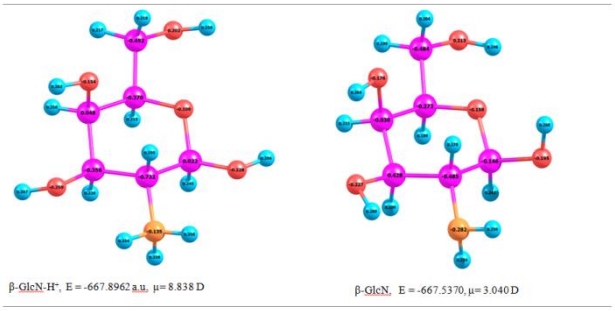

Fig. 6. Charge distribution in β-GlcN-H^+ and β-GlcN with energy minima (E) and dipole moments (μ).

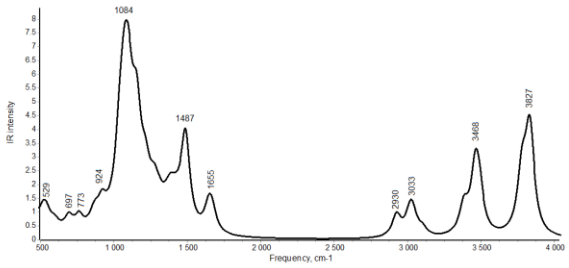

Fig. 7. Theoretical vibrational spectrum of β- GlcN-H^+ for gas.

The mechanism for cross-linking CHS with GA is presumed to involve the interaction of free amine groups of chitosan and with aldehydic groups of GA to form stable imine (C=N) bond [50] as shown in Scheme 1**.** The spectral changes in the macromolecule of CHS after cross-linking and protonation to PCCs is shown in Fig 8. A general decrease in the intensities of all peaks was observed in PCCs. CHS peaks at 640-671 cm^{-1} which were associated with ring C-C bending disappeared, this observation was also made for IR spectra of β-GlcN-H^+. The NH_2 vibration mode at 3435-3470 cm^{-1} also disappeared, signifying successful formation of Schiff base between GA and CHS. Preserved modes of amines, which are protonated in PCCs were seen at 3380 and 3406 cm^{-1}. The bands at 1165 and 1423 cm^{-1} representing C-O stretch and CH_2 bend respectively, weakened while characteristic NH_2 bending band at 1660 cm^{-1} became broader and stronger, associated with C=N mode after crosslinking. New peak at 1507 cm^{-1} was assigned to NH_3^+ bending and corresponded to bending mode of NH_3^+ observed in β-GlcN-H^+ at 1490 cm^{-1}.

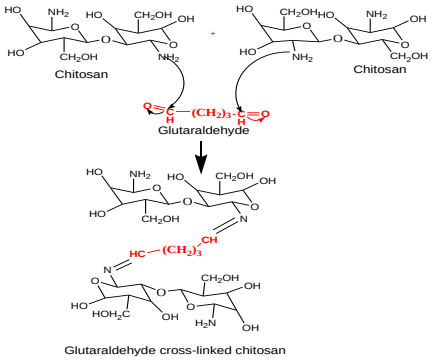

Scheme 1. Reaction mechanism for cross-linking chitosan with glutaraldehyde.

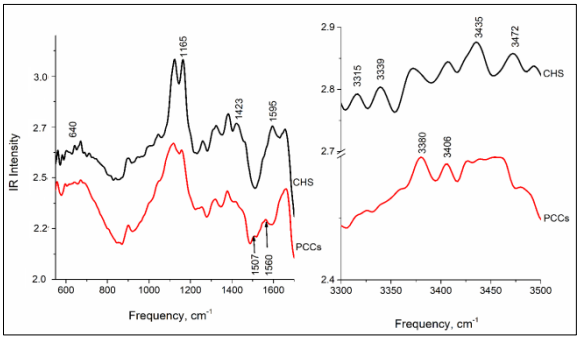

Fig. 8. Comparison of FT-IR spectra of PCCs and CHS.

3.3 Interaction of F^- with Chitosan

3.3.1 Fluorinated CHS and GlcN. Interaction of β-GlcN with F^- was modelled through chemical reaction:

$$\beta\text{-GlcN} + F^- \longrightarrow \beta\text{-GlcN-}F^- + \Delta rE \qquad (5)$$

F^- was 'placed' between NH_2 and OH group attached to C3. The H atom at that position represented the most electropositive atom in the molecule (Mulliken charge (q) = 0.289 a.u) as seen in Fig. 6. However, optimization directed F^- to the site between H9 of the amino group (q = 0.259 a.u) and H8 (q = 0.268 a.u) of OH group attached to C1 in the pyranose ring, which represents the highest combined electropositive site in the molecule, thus the most favorable for attachment.

Optimized structure of fluorinated adduct, β-GlcN-F is shown in Fig. 9 **(**embedded**)** and structural parameters are listed in Table 3**.** The energy of F^- attachment to β-GlcN (ΔrE) was calculated as ΔrE = -206 $kJmol^{-1}$. A slight change in the geometry of the molecules was observed, longer bond lengths and smaller bond angles compared to β-GlcN. IR spectrum of β-GlcN-F shown in Fig. 9, depicts an intense peak at 2107 cm^{-1} which was associated with stretching of OH----F bond. Another band identified in the adduct, which was absent in β-GlcN is 3275 cm^{-1} which signify stretching of intermolecular NH----F bond.

Table 3. Geometric parameters of the optimized structures of the β-GlcN adducts.

Parameter / Adduct	Bond lengths (Å) β-GlcN-F	β-GlcN-H^+	β-GlcN-HF
R(C1-C2)	1.544	1.530	1.535
R(C2- N1)	1.472	1.514	1.482
R(C3-O2)	1.430	1.425	1.417
R(O2-H11)	0.975	0.965	0.973
R(C1-O4)	1.450	1.378	1.409
R(C1- O1)	1.426	1.393	1.398
R(O1-H8)	1.067	0.966	0.964
R(C4-O3)	1.426	1.413	1.417
R(O3-H12)	0.967	0.964	0.967
R(H8……F1)	1.362	-	-
R(H9…..F1)	1.911	-	-
R(N1…..H10)	-	-	1.538
R(H10-F1)	-	-	0.996
R(H11…..F1)	-	-	1.833
Bond angles (°)			
A(C1-C2-N1)	115.8	111.1	111.1
A(C3-O2-H11)	102.5	110.9	111.8
A(C1-O1-H8)	103.9	110.5	108.7
A(C4-O3-H12)	105.2	109.9	106.3
A(O4-C5-C6)	105.6	106.9	106.5
A(C1-O4-C5)	113.4	113.6	112.8
A(O1-C1-O4)	109.0	111.2	108.9
A(O1-H8-F1)	166.9	-	-
A(H20-F1-H21)	83.7	-	-
A(N1…H10 –F1)	-	-	168.9
A(H10-F1…..H11)	-	-	82.3
Dihedral angles(°)			
D(C2-C1-O1-H8)	-78.9	-175.6	-176.7
D(C2-C3-C4-C5)	50.2	55.3	48.7
D(O4-C5-C6-O5)	55.2	67.8	62.6
D(O1-H8_F26_H21)	-26.8	-	-
D(C2-N1...H10-F1)	-	-	38.8
D(N1….H10-F1…..H11)	-	-	73.6

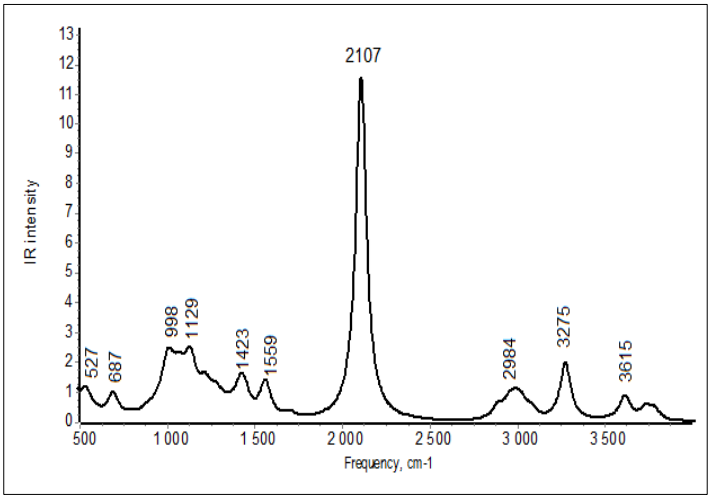

Fig. 9. Theoretical IR spectrum of F-β-GlcN and structure of F- GlcN (embedded).

3.3.2 Fluorinated GlcN-H$^+$ and PCCs. Results of F$^-$ adsorption from water using CHS in pristine and modified from are shown in Table 4. Adsorption in CHS powder and cross-linked chitosan (CCs) gave efficiencies below 20% with very low adsorption capacities (0.2-0.4 mg/g). PCCs, on the other hand recorded a significantly higher efficiency, 77% and adsorption capacity of 1.6 mg/g. This efficiency is considered useful in decontamination of water with F$^-$ concentration below 10 mgF/L.

Table 4: Fluoride adsorption efficiency (%) and capacity (Qe) for CHS, CCs and PCCs.

Adsorbent	Final pH	C_e (mg/L)	% F-adsorbed	Q_e, (mg/g)
CHS	6.17	9.20	11.50	0.25
CCs	6.25	8.40	19.20	0.40
PCCs	6.00	2.40	77.00	1.60

Initial F$^-$ (C_0) in water =10.4 mg/L and initial pH of water = 7.2.

In the theoretical model, the most favorable site for attachment of F$^-$ to β-GlcN-H$^+$ was between NH10 and OH1. A sigma bond was formed between H$^+$ and F$^-$, forming HF molecule which is attached to glucosamine via OH----F and FH----N hydrogen bonding (Fig. 10-embedded). Again, the position of attachment has the highest combined electropositivity in the molecule. Selected structural parameters are listed in Table 3. The energy of attaching F$^-$ to β-GlcN-H$^+$ was calculated as ΔrE= - 676 kJ mol^{-1}, which is about 3 times lower in magnitude compared to attaching F$^-$ to β-GlcN. This means that it is much easier to attach F$^-$ to β-GlcN-H$^+$. This observation is well supported by experimental data in Table 4, which show that PCCs adsorbed 4 times more F$^-$ in aqueous solution than unprotonated CCs. IR spectrum of β-GlcN-HF (Fig. 10) show shift to longer wavenumbers, in the bands related to presence F$^-$ in the molecules compared to unptotonated adduct. The N----HF band is observed at 2602 cm^{-1} and OH----F stretching band at 3660 cm^{-1}, in β-GlcN-F the two bands are seen at 2107 and 3275 cm^{-1} respectively.

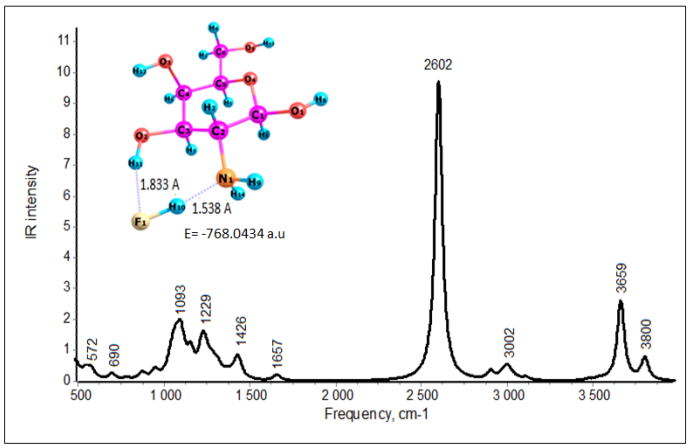

Fig. 10. Theoretical IR spectrum of β-GlcN-HF and optimized structure of the adduct (**embedded**).

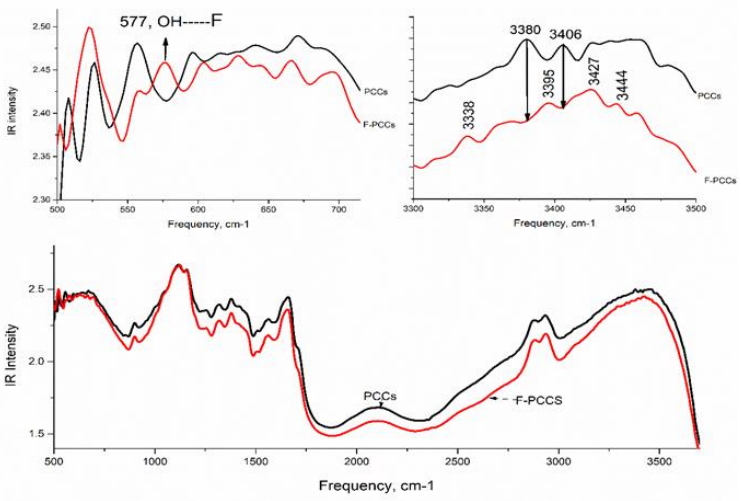

Fig. 11. Comparison of FT-IR spectra of F-PCCs and PCCs.

Table 5. Selected frequencies (cm^{-1}) of fluorinated PCCs and GlcN molecule.

F-PCCS- Expt. freq. (cm^{-1})	GlcN-HF-DFT/B3lYP freq. (cm^{-1})	Vibration modes
577	572	OH….F bending
693	690	C-C-C ring bending
1123	1126	N…..HF bending.
1156	1154	C-O-C stretching
1315	1318	CH_2 bending
1659	1657	C=O stretching/N-H_2 bending
-	2602	N…..HF stretching
2941	3002	C-H stretching
3338	-	N….HF stretching
3424	3471	N-H symmetric stretching

4. CONCLUSIONS

Chitosan molecule in crystalline phase may exist as α- or β-copolymer of $_D$-GlcN. According to our DFT calculations, the β-form has lower energy in the potential energy surface (PES) and is thus considered to be more stable. Calculated geometrical parameters, vibrational frequencies and the electronic absorption spectrum of β-D-GlcN molecule were found to correspond well with those observed in the XRD structure, FT-IR modes and UV-Vis spectrum of CHS. When it comes to chitosan interaction with F$^-$, PCCs was found to possess higher F$^-$ adsorption capacity than CHS and CCs. Analysis by DFT also confirmed that protonated β-GlcN had a better ability to bind F$^-$ than its unprotonated form. The electropositivity of H atoms attached to NH_2 and OH functional groups and the dipole moment of the molecule highly influenced the efficiency of F$^-$ attachment. FT-IR analysis of F$^-$

treated PCCs showed the presence of hydrogen bonds; OH----F in lower frequency region and H_2N---HF bands in higher frequency region (3330-3450 cm^{-1}). Similar bands were also seen in theoretical IR spectrum of β-GlcN-HF adduct. Experimental and theoretical results in this work show that protonation of the amine groups of chitosan is highly effective in improving its capacity to decontaminate F^- polluted water. The result demonstrates that the OH and NH_2 functional groups of chitosan work together for effective binding of F^- from solution.

5. REFERENCES

[1] Ban Z., Horev B., Rutenberg R., Danay O., Bilbao C., McHugh T., Rodov V., Poverenov E., Efficient production of fungal chitosan utilizing an advanced freeze-thawing method; quality and activity studies, *Food Hydrocolloids*, 81, 380-388, **2018**.

[2] Goy R.C., Morais S.T.B., Assis O.B.G.,R.C. Goy, S.T.B. Morais, O.B.G. Assis, Evaluation of the antimicrobial activity of chitosan and its quaternized derivative on E. coli and S. aureus growth, *Revista Brasileira de Farmacognosia*, 26, 122-127, **2016.**

[3] Ewis M., Elkholy S.S., Elsabee M.Z.,M. Eweis, S.S. Elkholy, M.Z. Elsabee, Antifungal efficacy of chitosan and its thiourea derivatives upon the growth of some sugar-beet pathogens, *International Journal of Biological Macromolecules*, 38, 1-8, **2006.**

[4] Xie Y., Li S., Wang F., Liu G.,Y. Xie, S. Li, F. Wang, G. Liu, Removal of perchlorate from aqueous solution using protonated cross-linked chitosan, *Chemical Engineering Journal*, 156, 56-63**, 2010.**

[5] Jaafari K., Ruiz T., Elmaleh S., Coma J., Benkhouja K.,K. Jaafari, T. Ruiz, S. Elmaleh, J. Coma, K. Benkhouja, Simulation of a fixed bed adsorber packed with protonated cross-linked chitosan gel beads to remove nitrate from contaminated water, *Chemical Engineering Journal*, 99, 153-160, **2004.**

[6] Huang R., Yang B., Liu Q., Gong N.,R. Huang, B. Yang, Q. Liu, N. Gong, Adsorption of a model anionic dye on protonated crosslinked chitosan, *Desalination and Water Treatment*, 52, 7693-7700, **2014.**

[7] Yong S.K., Shrivastava M., Srivastava P., Kunkhikrishnan A., Bolan N., S.K. Yong, M. Shrivastava, P. Srivastava, A. Kunhikrishnan, N. Bolan, Environmental Applications of Chitosan and Its Derivatives, in: D.M. Whitacre, (Ed.) *Reviews of Environmental Contamination and Toxicology* Volume 233, Springer International Publishing, Cham, pp. 1-43,. **2015.**

[8] Souza V. C., Dotto G. L., Application of chitosan based materials as edible films and coatings, in: Dotto L., Campana-Filho S., Pinto L., (Eds). *Frontiers in biomaterials: Chitosan based materials and its applications*, Volume 3, pp. 249-271, **2017**.

[9] Wang H., Qian J., Ding F., Emerging chitosan-based films for food packaging applications, *Journal of agricultural and food chemistry*, 66, 395-413, **2018.**

[10] Asghari F., Samiei M., Adibkia K., Akbarzadeh A., Davaran S., Biodegradable and biocompatible polymers for tissue engineering application: A review, *Artificial cells, nanomedicine, and biotechnology*, 45, 185-192, **2017.**

[11] Terreux R., Domard M., Viton C., Domrad A., R. Terreux, M. Domard, C. Viton, A. Domard, Interactions Study between the Copper II Ion and Constitutive Elements of Chitosan Structure by DFT Calculation, *Biomacromolecules*, 7, 31-37, **2006.**

[12] Miretzky P., Cirelli A.F., P. Miretzky, A.F. Cirelli, Fluoride removal from water by chitosan derivatives and composites: A review, *Journal of Fluorine Chemistry*, 132, 231-240, **2011.**

[13] WHO, Guidelines for Drinking-water Quality, in, **2011**.

[14] Islam M., Patel R., M. Islam, R. Patel, Thermal activation of basic oxygen furnace slag and evaluation of its fluoride removal efficiency, *Chemical engineering journal*, 169, 68-77, **2011.**

[15] Mohapatra M., Anand S., Mishra B.K., Giles D.E., Singh P.,M. Mohapatra, S. Anand, B.K. Mishra, D.E. Giles, P. Singh, Review of fluoride removal from drinking water, *Journal of environmental management*, 91, 67-77. **2009.**

[16] Khairnar M.R., Dodamani A.S., Jadhav H.C., Naik R.G., Deshmukh M.A., M.R. Khairnar, A.S. Dodamani, H.C. Jadhav, R.G. Naik, M.A. Deshmukh, Mitigation of Fluorosis - A Review, *Journal of Clinical and Diagnostic Research : JCDR*, 9, ZE05-ZE09, **2015.**

[17] Dubey S., Agarwal M., Gupta A., Recent developments in defluoridation of drinking water in India, in: Singh V., Yadav S., Yadava R. (eds) *Environmental Pollution. Water Science and Technology Library*, volume 77. Springer, Singapore, pp 345-356, **2018.**

[18] Viswanathan N., Sundaram C.S., Meenakshi S.,N. Viswanathan, C.S. Sundaram, S. Meenakshi, Sorption behaviour of fluoride on carboxylated cross-linked chitosan beads, *Colloids and Surfaces B: Biointerface*s, 68, 48-54 **2009**.

[19] Chen A.H., Chen S.M., Biosorption of azo dyes from aqueous solution by glutaraldehyde-crosslinked chitosans, *Journal of Hazardous Materials*, 172, 1111–1121, **2009.**

[20] Abraham S., Rajamanickam D., Srinivasan B., Preparation, characterization and cross-linking of chitosan by microwave assisted synthesis, *Science International*, 6, 18-30, **2018**.

[21] Huang R., Yang B., Liu Q., Ding K.,R. Huang, B. Yang, Q. Liu, K. Ding, Removal of fluoride ions from aqueous solutions using protonated cross-linked chitosan particles, *Journal of Fluorine Chemistry*, 141, 29-34, **2012.**

[22] Viswanathan N., Sundaram C.S., Meenakshi S., Removal of fluoride from aqueous solution using protonated chitosan beads, *J Hazard Mater*, 161, 423-430, **2009.**

[23] Thakre D., Jagtap S., Bansiwal A., Labhsetwar N., Rayalu S., Synthesis of La-incorporated chitosan beads for fluoride removal from water, *Journal of Fluorine Chemistry*, 131, 373-377, **2010.**

[24] Jagtap S., Thakre D., Wanjari S., Kamble S., Labhsetwar N., Rayalu S., New modified chitosan-based adsorbent for defluoridation of water, *Journal of Colloid and Interface Science*, 332, 280-290, **2009.**

[25] Liang P., Zhang Y., Wang D., Xu Y., Luo L., Preparation of mixed rare earths modified chitosan for fluoride adsorption, *Journal of Rare Earths*, 31, 817-822, **2013**.

[26] Marwa E., Quantum chemical study of sodium cation and fluoride anion attachment to the chitosan constituents in: Materail Science, *Nelson Mandela African Institition of Science and Technology*, **2016.**

[27] de Queiroz Antonino R.S.C.M., Lia Fook B.R.P., de Oliveira Lima V.A., de Farias Rached R.Í., Lima E.P.N., da Silva Lima R.J., Peniche Covas C.A., Lia Fook M.V., Preparation and Characterization of Chitosan Obtained from Shells of Shrimp (Litopenaeus vannamei Boone), *Marine drugs*, 15. 141, **2017.**

[28] Sagheer F.A.A., Al-Sughayer M.A., Muslim S., Elsabee M.Z., Extraction and characterization of chitin and chitosan from marine sources in Arabian Gulf, *Carbohydrate polymers*, 77, 410-419, **2009.**

[29] Altomare A., Cuocci C., Giacovazzo C., Moliterni A., Rizzi R., Corriero N., Falcicchio A., EXPO2013: a kit of tools for phasing crystal structures from powder data, *Journal of Applied Crystallography*, 46, 1231-1235, **2013.**

[30] Abdou E.S., Nagy K.S., Elsabee M.Z., Extraction and characterization of chitin and chitosan from local sources, *Bioresource technology*, 99, 1359-1367, **2008.**

[31] Brugnerotto J., Lizardi J., Goycoolea F.M., Argüelles-Monal W., Desbrières J., Rinaudo M., An infrared investigation in relation with chitin and chitosan characterization, *Polymer*, 42, 3569-3580, **2001.**

[32] Bertoni F. A., González J. G., García S. I., Sala L.F., Bellú S. E., Application of chitosan in removal of molybdate ions from contaminated water and groundwater, *Carbohydrate polymers*, 180, 55-62, 2018.

[33] Hanwell M., Curtis D., Lonie D., Vandermeersch T., Zurek E., Hutchison G., Avogadro: an advanced semantic chemical editor, visualization, and analysis platform, *Journal of Cheminformatics*, 4, 17, **2017.**

[34] Granovsky A.A., Firefly version 8.1.1 http://classic.chem.msu.su/gran/firefly/index.html in, **2008.**

[35] K.K.B. Michael W. Schmidt, Jerry A. Boatz, Steven T. Elbert, Mark S. Gordon, Jan H. Jensen, Shiro Koseki, Nikita Matsunaga, Kiet A. Nguyen, Shyjun SU, Theresa L. Windus, Michel Dupuis and John A. Montgomery, General atomic and molecular electronic structure system, in: *Journal of Computational Chemistry*, pp. 1347-1363, **1993.**

[36] Becke A.D., Density-functional thermochemistry. III. The role of exact exchange, *The Journal of Chemical Physics*, 98, 5648-5652, **1993.**
[37] Perdew J.P., Density-functional approximation for the correlation energy of the inhomogeneous electron gas. *Physical Review B*, 33, 8822, **1986.**
[38] Medina F.E., Neves R.P., Ramos M. J., Fernandes P. A., A QM/MM study of the reaction mechanism of human β-ketoacyl reductase, *Physical Chemistry Chemical Physics*, 19, 347-355, **2017.**
[39] Zhurko G.A., ChemCraft 1.8 in, http://www.chemcraftprog.com, **2017.**
[40] Naito P.K., Ogawa Y., Kimura S., Iwata T., Wada M., Crystal transition from hydrated chitosan and chitosan/monocarboxylic acid complex to anhydrous chitosan investigated by X-ray diffraction, *Journal of Polymer Science Part B: Polymer Physics*, 53, 1065-1069, **2015.**
[41] Wang X., Ding M., Liu Z., Wang D., Synthesis of a chitosan-based functional biopolymer with both catalytic and binding groups for protein and DNA hydrolysis, *RSC Advances*, 5, 19541-19551, **2015.**
[42] Rahangdale D., Kumar A., Derivatized chitosan: fundamentals to applications, in: *Biopolymer grafting*, Elsevier, pp. 251-284, **2018**.
[43] Lertworasirikul A., Yokoyama S., Noguchi K., Ogawa K., K. Okuyama, Molecular and crystal structures of chitosan/HI type I salt determined by X-ray fiber diffraction, *Carbohydrate Research*, 339, 825-833, **2004.**
[44] Peña I., Kolesniková L., Cabezas C., Bermúdez C., Berdakin M., Simão A., Alonso J.L., The shape of D-glucosamine, *Physical Chemistry Chemical Physics*, 16, 23244-23250, **2014.**
[45] Delbianco M., Kononov A., Poveda A., Yu Y., Diercks T., Jiménez-Barbero J., Seeberger P. H., Well-defined oligo- and polysaccharides as ideal probes for structuralstudies, *Journal of the American Chemical Society*, 140, 5421-5426, **2018.**
46] Zając A., Hanuza J., Wandas M., Dymińska L., Determination of N-acetylation degree in chitosan using Raman spectroscopy, *Spectrochimica Acta Part A: Molecular and Biomolecular Spectroscopy*, 134, 114-120, **2015.**
[47] Ghimire S., Neupane B., Pokhrel S., Le H., Lebek W., Heinrich G., Yadav P., Adhikari R., Conversion of chitin isolated from fresh-water prawns to chitosan and its characterization, *Polymers Research Journal*, 11, 1-15, **2017.**
[48] Liu D., Wei Y., Yao P,, Jiang L., Determination of the degree of acetylation of chitosan by UV spectrophotometry using dual standards, *Carbohydr Res*, 341, 782-785, **2006.**
[49] Fatahi A., Ghorat M., Pourjavadi A, Kord T., Torabi A., DFT/B3LYP study of thermochemistry of d-glucosamine, a representative polyfunctional bioorganic compound, *Scientia Iranica*., 15, 422-429, **2008.**
[50] Mikhailov S. N., Zakharova A. N., Drenichev M. S., Ershov A. V., Kasatkina M. A., Vladimirov L. V., Novikov V. V., Kildeeva N. R., Crosslinking of chitosan with dialdehyde derivatives of nucleosides and nucleotides. Mechanism and comparison with glutaraldehyde, *Nucleosides, nucleotides and nucleic acid*s, 35, 114-129, **2016.**

6. ACKNOWLEDGEMENTS

This project has received funding from the European Union's Horizon 2020 research and innovation program under grant agreement Number 690378. The authors are also thankful to Mwalimu Nyerere African Union Scholarship Scheme (MNAUSS) for the award of fellowship to Agatha Wagutu.